PROCEEDINGS OF SCIENCE

$\pi\pi$ scattering and $\gamma\gamma \to \pi\pi$ in SU(2) χPT augmented by a light scalar

Arbin Thapaliya*
Department of Chemistry and Physics, Franklin College, Franklin, Indiana 46131, USA
E-mail: AThapaliya@franklincollege.edu

Daniel R. Phillips
Institute of Nuclear and Particle Physics and Department of Physics and Astronomy, Ohio University, Athens, Ohio 45701, USA
Institut für Kernphysik, Technische Universität Darmstadt, 64289 Darmstadt, Germany
ExtreMe Matter Institute EMMI, GSI Helmholtzzentrum für Schwerionenforschung GmbH, 64291 Darmstadt, Germany
phillid1@ohio.edu

The lowest-lying resonance in the QCD spectrum is the 0^{++} isoscalar σ meson, also known as the $f_0(500)$. We augment SU(2) chiral perturbation theory (χPT) by including the σ meson as an additional explicit degree of freedom, as proposed by Soto, Talavera, and Tarrús and others. In this effective field theory, denoted χPT_S, the σ meson's well-established mass and decay width are not sufficient to properly renormalize its self energy. At $\mathcal{O}(p^4)$ another low-energy constant appears in the dressed σ-meson propagator; we adjust it so that the isoscalar pion-pion scattering length is also reproduced. We compare the resulting amplitudes for the $\pi\pi \to \pi\pi$ and $\gamma\gamma \to \pi\pi$ reactions to data from threshold through the energies at which the σ-meson resonance affects observables. The leading-order (LO) $\pi\pi$ amplitude reproduces the σ-meson pole position, the isoscalar $\pi\pi$ scattering lengths and $\pi\pi$ scattering and $\gamma\gamma \to \pi\pi$ data up to $\sqrt{s} \approx 0.5$ GeV. It also yields a $\gamma\gamma \to \pi\pi$ amplitude that obeys the Ward identity. The value obtained for the π^0 polarizability is, however, only slightly larger than that obtained in standard χPT.

The 9th International workshop on Chiral Dynamics
17-21 September 2018
Durham, NC, USA

*Speaker.

PoS(CD2018)087

1. Introduction

The spectrum of Quantum Chromodynamics (QCD) consists of several bound and resonant states with masses below 1 GeV. The lightest QCD bound states are the pseudoscalar pions, which have a special role in the theory as pseudo-Nambu-Goldstone bosons of QCD's approximate, spontaneously-broken, chiral symmetry. The lowest-lying QCD resonance has 0^{++} quantum numbers: the same as those of the vacuum. This state, often termed the "σ meson", and also referred to as the $f_0(500)$, is (slightly) manifested in pion-pion scattering. It has attracted much attention over many years. We do not review that history here, instead referring the interested reader to Ref. [1].

Determinations of σ-meson parameters rely on an extrapolation of the $\pi\pi$ scattering amplitude into the complex plane: one must obtain its mass, M_σ, and width, Γ, from the position in the complex energy plane at which a pole in the $\pi\pi$ t-matrix occurs. From 1996–2010 the Particle Data Group (PDG) [2] results for the mass and decay width ranged from 400 to 1200 MeV and from 500 to 1000 MeV, respectively. These wide variations occurred because obtaining the mass, decay width, and couplings of this resonance is difficult: the resonance is very broad and can hardly be seen in the $\pi\pi$ scattering phase shifts. The standard Breit-Wigner formulation for narrow resonances is definitely not applicable in this case. The last fifteen years has seen the advent of dispersion-relation evaluations that incorporate the constraints of chiral symmetry and—in some cases—crossing symmetry too [3, 4, 5, 6]. The results of these calculations largely agree, and the 2015 review of Peláez quotes a σ-meson pole position [1]:

$$\sqrt{s} = M_\sigma - i\Gamma/2; \quad M_\sigma = (449^{+22}_{-16})\ \text{MeV}; \quad \Gamma = (550 \pm 24)\ \text{MeV}. \tag{1.1}$$

This pole position is markedly lower than the scale of chiral-symmetry breaking, $\Lambda_{\chi\text{SB}}$, usually understood to be the rho-meson mass, or $4\pi F$, with $F = 92.419$ MeV the pion decay constant. It is also comparable to the kaon mass. Together with findings from lattice QCD at large N_f, this has led some authors to explore EFTs in which the σ is a dilaton of QCD (see, e.g., Refs. [7, 8]).

Regardless of whether the scalar excitation is a QCD dilaton or not, $|M_\sigma - i\Gamma/2|$ is well below $\Lambda_{\chi\text{SB}}$, so the 0^{++} resonance can be expected to spoil the convergence of the χPT expansion in channels where it plays a role. This motivates augmenting standard chiral perturbation theory by the addition of a σ field, whose mass is between the pseduo-Goldstone-boson mass scale, M_π, and $\Lambda_{\chi\text{SB}}$. The resulting EFT has (spontaneously and dynamically broken) $\text{SU}(2)_L \times \text{SU}(2)_R$ symmetry. It was written down by Soto, Talavera, and Tarrús in Ref. [9], who called it χPT_S. It has also been explored in Refs. [10, 11]. In χPT_S the σ is not a Goldstone boson of QCD, so its couplings must be fixed from data: only a few are constrained by chiral symmetry.

Here we examine the reactions $\pi\pi \to \pi\pi$ and $\gamma\gamma \to \pi\pi$, both of which couple to the 0^{++} channel in the s-channel, and exhibit slow convergence when investigated in two-flavor χPT. We compare those standard χPT calculations at leading [$\mathcal{O}(p^2)$] order to χPT_S at LO: the theory with the additional scalar isoscalar degree of freedom intercalates between χPT at $\mathcal{O}(p^2)$ and χPT at $\mathcal{O}(p^4)$. We demonstrate that χPT_S naturally includes a σ meson with a large width that is, nonetheless, not prominent in the $\pi\pi$ S-wave phase shift.

In our approach, we employ a power counting with two light scales: m_π and M_σ. The resulting hierarchy on which the EFT is built is then $m_\pi \ll M_\sigma \ll \Lambda_{\chi\text{SB}}$. The LO amplitude in our approach

consists of the standard χPT $\mathcal{O}(p^2)$ interaction plus an s-channel σ pole that is enhanced near the resonance so it becomes $\mathcal{O}(p^0)$. (Away from $s \sim M_\sigma^2$ the s-channel pole is $\mathcal{O}(p^4/M_\sigma^2)$.)

The rest of this paper is structured as follows: in Sec. 2 we review the Lagrangian developed in Ref. [9] (or, equivalently, the later Ref. [11]), and explain the power counting we use in this paper. In Sec. 3 we calculate the σ propagator at $\mathcal{O}(p^4)$. In Sec. 4 we employ this propagator, together with the standard mechanisms of χPT at $\mathcal{O}(p^2)$, to describe $\pi\pi$ scattering. In Sec. 5 we consider $\gamma\gamma \to \pi\pi$. Sec. 6 offers our conclusions.

2. The Lagrangian and Power counting

In Ref. [9] Soto *et al.* modified the χPT Lagrangian to χPT_S by including terms containing a dynamic isosinglet scalar σ field S in addition to the matrix U that parameterizes the Goldstone boson fields in standard SU(2) χPT [12]. In the notation of Ref. [9] the terms in the effective Lagrangian that are relevant for this study are:

$$\begin{aligned}\mathscr{L}_2^S = &\left(\frac{F^2}{4} + F c_{1d} S + c_{2d} S^2 + \cdots\right)\langle D_\mu U (D^\mu U)^\dagger\rangle + \left(\frac{F^2}{4} + c_{1m} S + c_{2m} S^2 + \ldots\right)\langle \chi U^\dagger + U\chi^\dagger\rangle \\ &+ \frac{1}{2}\partial_\mu S \partial^\mu S - \frac{1}{2} m_S^2 S S - f_{2p}(\partial_\mu \partial^\mu S)^2 - \frac{\lambda_3}{3!} S^3 - \frac{\lambda_4}{4!} S^4 \,, \end{aligned} \tag{2.1}$$

where c_{1d}, c_{2d}, c_{1m}, c_{2m}, and f_{2p} are new low-energy constants (LECs) in the $\mathcal{O}(p^2)$ Lagrangian. In Eq. (2.1), $D_\mu U = \partial_\mu U - i[v_\mu, U] + i\{a_\mu, U\}$ is the chiral covariant derivative, χ represents a scalar source. The terms on the second line are the Lagrangian of the scalar S field with bare mass m_S. This Lagrangian, unlike the typical $\mathscr{L}$ for scalar fields, contains an additional fourth-order term. Although nominally fourth order this term is needed for proper renormalization of the σ-meson self energy. We argue that this term is important for the phenomenology of the σ, since in its absence the σ couples strongly to two pions, causing the bumps in the $\pi\pi \to \pi\pi$ and $\gamma\gamma \to \pi\pi$ processes to be very pronounced—something that is not seen in data.

In χPT_S we consider two different energy regions of interest. In the near-threshold region we have $p \sim m_\pi$ and the standard χPT power counting: each vertex with n powers of momentum p or m_π scales as p^n and the pion propagator scales as p^{-2}. In this regime the σ propagator scales as m_S^{-2}, since p is markedly less than m_S. It therefore produces larger threshold effects than the χPT counter terms at $\mathcal{O}(p^4)$, since m_S is taken to be $\ll \Lambda_{\chi\text{SB}}$.

But the effects of the σ are enhanced—to an effect that is nominally larger than the $\mathcal{O}(p^2)$ leading χPT $\pi\pi$ amplitude—in the second regime where $p \sim m_S$, i.e., in the vicinity of the resonance. Here the σ propagator develops a pole. It then needs to be dressed by the inclusion of the leading $[\mathcal{O}(p^4)]$ self energy, Σ, which is resumed to all orders in the s-channel via a Dyson equation. The inclusion of f_{2p} as part of this self energy is mandatory for proper renormalization, which is why this particular p^4 operator is relevant in our leading-order study. The renormalized Σ ensures that the σ develops a pole at the physical mass and width. There is then a (in principle narrow) kinematic window where the $p^2 - M_\sigma^2$ piece of the inverse σ propagator is of the same order, or smaller than, the $\mathcal{O}(p^4)$ self energy. In this kinematic window the resumed σ propagator scales as p^{-4}, is enhanced, and becomes a leading-order effect.

3. Calculation of the σ-meson self energy

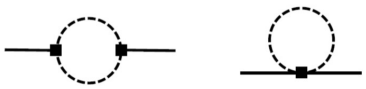

Figure 1: The self-energy diagrams of the σ meson at the one-pion-loop level, i.e. $\mathcal{O}(p^4)$. The solid (dashed) line represents the $\sigma(\pi)$ propagator. The squares indicate that the interaction appears due to the terms containing the S field in the $\mathscr{L}_2^S$ Lagrangian. The left-hand diagram involves two insertions of c_{1d} and the right-hand one one insertion of c_{2d} or c_{2m}.

We have performed a calculation of the σ-meson self energy to $\mathcal{O}(p^4)$ in Ref. [13]. Only one-loop diagrams need to be considered and the pertinent ones are shown in Fig. 1. We can express the σ self energy in the modified minimal-subtraction ($\overline{MS}$) renormalization scheme as

$$\Sigma^{\overline{MS}}(s,\mu) \;=\; \Sigma_0(\mu) + \Sigma_1(\mu)s + \Sigma_2(\mu)s^2 + c_{1d}^2(\mu)\tilde{\Sigma}(s)\;, \tag{3.1}$$

where μ is a renormalization scale.

In Eq. (3.1), the bare constants Σ_0, Σ_1, and Σ_2 are μ-dependent whereas $\tilde{\Sigma}(s)$ is independent of μ. When Eq. (3.1) is combined with bare propagators and vertices the $\Sigma_0(\mu)$-term is renormalized by $m_S^2(\mu)$ and the term linear in s by $c_{1d}^2(\mu)$. However, the left-hand graph in Fig. 1 is quartically divergent, and so there is also an $s^2\ln(\mu)$ piece of the diagram that must be absorbed by a counterterm. This is done by $f_{2p}(\mu)$. We then express the dressed renormalized σ propagator as

$$iD(s) \;=\; \frac{i}{s - m_{S,r}^2 - 2f_{2p,r}s^2 - c_{1d,r}^2\tilde{\Sigma}(s)}\;, \tag{3.2}$$

where the quantities with subscripts r are the μ-independent renormalized quantities. Bruns also observed the presence of the $s^2\ln(\mu)$ term that we found here [14], but then discarded it and did not explore its consequences for σ phenomenology.

Equation (3.2) shows that there are three unknown parameters—$m_{S,r}$, $f_{2p,r}$, and $c_{1d,r}$—that affect σ-meson physics at leading order in $\chi\mathrm{PT}_S$. Two constraints on them are obtained by demanding that the quadratic s-dependence $\sim f_{2p,r}$ and the s-dependence of $\tilde{\Sigma}(s)$ in Eq. (3.2) ultimately produce a pole at the position (1.1). The third constraint results from demanding that the LO amplitude reproduce the experimental pion-pion scattering length in the scalar-isoscalar channel, a_0^0=0.2210(47)(40) m_π^{-1} [15]. (For details, see Ref. [13].) Here, and throughout, we take $m_\pi = 139.57$ MeV [2]. The values of $m_{S,r}$, $f_{2p,r}$, and $c_{1d,r}$ we then obtain are

$$m_{S,r} = 221^{+5}_{-4}\ \mathrm{MeV};\quad c_{1d,r} = 0.206^{+0.001}_{-0.002};\quad f_{2p,r} = (3.4^{+0.01}_{-0.02})\times 10^{-6}\ \mathrm{MeV}^{-2}. \tag{3.3}$$

The errors are purely from the propagation of uncertainties on input quantities, and do not include the effect of higher-order terms. These are the $\chi\mathrm{PT}_S$ parameters for the particular set of renormalization conditions we chose: other renormalization conditions are certainly possible.

In Ref. [9], Soto *et al.* pointed out the need for renormalization of the one-loop σ self energy, but they set the finite part of f_{2p} to zero. We find a non-zero, but natural, value: $f_{2p,r} \sim 1/\Lambda_{\chi\mathrm{SB}}^2$. Also, our analytic result for the self energy $\tilde{\Sigma}$ agrees with that found in Ref. [9]. The key difference to our result is that we corrected a factor-of-two error in the relation between the width and self energy that is present in both Refs. [9, 11].

4. S-wave pion-pion scattering at leading order in χPT_S

We now compute $\pi\pi \to \pi\pi$ and the relevant diagrams are shown in Fig. 2. The thick line indicates that we have resummed the σ self energy and so are employing the propagator (3.2) in all three diagrams. However, diagrams (iii) and (iv) are formally next-to-leading order (NLO), $\mathcal{O}(p^4/M_\sigma^2)$ and are numerically small.

In contrast, the LO mechanisms are diagram (ii)—the tree-level χPT $\pi\pi$ scattering amplitude—near threshold, where it is $\mathcal{O}(p^2)$, and diagram (i)—the s-channel σ pole—in the resonance region, where it is $\mathcal{O}(p^0)$. By combining diagrams (i) and (ii) we obtain an amplitude that is LO in both the threshold and resonance regions, and interpolates smoothly between the two.

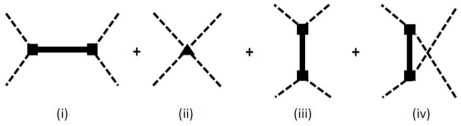

Figure 2: Tree-level diagrams contributing to $\pi\pi$ scattering in χPT_S: (i) s-channel, (ii) contact term, (iii) t-channel, and (iv) u-channel. The triangle represents the interaction from the standard χPT $\mathscr{L}_2$ Lagrangian. The thick solid line indicates the dressed σ propagator of Eq. (3.2). The first two diagrams form the LO amplitude in our calculation, while the other two are part of the NLO amplitude.

The isospin I=0 projected pion-pion scattering amplitude at LO is then

$$T^{I=0}(s,t,u) = \frac{1}{F^2}\left(3(s-m_\pi^2)+(t-m_\pi^2)+(u-m_\pi^2) - \frac{12c_{1d,r}^2(s-2m_\pi^2)^2}{s-m_{S,r}^2-2f_{2p,r}s^2-c_{1d,r}^2\tilde{\Sigma}(s)}\right). \quad (4.1)$$

This amplitude is only perturbatively unitary: diagram (i) is unitary on its own, but no loop effects associated with diagram (ii) are included in our LO calculation, they enter only at $\mathcal{O}(p^4/\Lambda_{\chi\mathrm{SB}}^2)$ in the chiral expansion, see also the discussion of the breakdown of this EFT below. Given this, we must use the first-order relation between the S-wave $\pi\pi$ phase shift δ_0^0 and $T^{I=0}$:

$$\delta_0^0 = \frac{|\mathbf{k}|}{32\pi\sqrt{s}}\int_{-1}^{1} d(\cos\theta)\ \Re[T^{I=0}(s,\cos\theta)]\ , \quad (4.2)$$

where $|\mathbf{k}|=\sqrt{s-4m_\pi^2}/2$ and θ are the center-of-mass (CM) momentum and scattering angle.

Figure 3 shows the standard LO χPT [$\mathcal{O}(p^2)$] result (dashed purple curve) and the total LO χPT_S phase shift (dash-dotted blue curve). The contributions from σ-meson physics are generally smaller than the $\mathcal{O}(p^2)$ χPT result. The s-channel σ-meson pole only affects the total $\pi\pi$ phase shift weakly. In Fig. 3 we also compare our LO result to the dispersive/Roy-equation analyses from Refs. [4, 16] (solid green and brown curves). And we display $\pi\pi$ phase-shift data. The left panel emphasizes the lower-energy range, where data (red circles) were obtained by analyzing the $\pi\pi$ scattering in the final-state interactions between pions in the K_{e4} decay $K^\pm \to \pi^\pm\pi^\mp e^\pm \nu$ [15]. The description of these near-threshold data is very good—especially considering this is only a LO calculation: adding the s-channel σ-meson pole ameliorates the discrepancy between the $\mathcal{O}(p^2)$ χPT result and the data. This σ mechanism does not affect the $I=2$ channel, so the good agreement of LO χPT with data there (not shown) is maintained.

In the right panel we compare to data (black squares) in the energy range above 500 MeV from Ref. [17], obtained from analysis of the reactions $\pi^+ p \to \pi^+\pi^-\Delta^{++}$ and $\pi^+ p \to K^+K^-\Delta^{++}$.

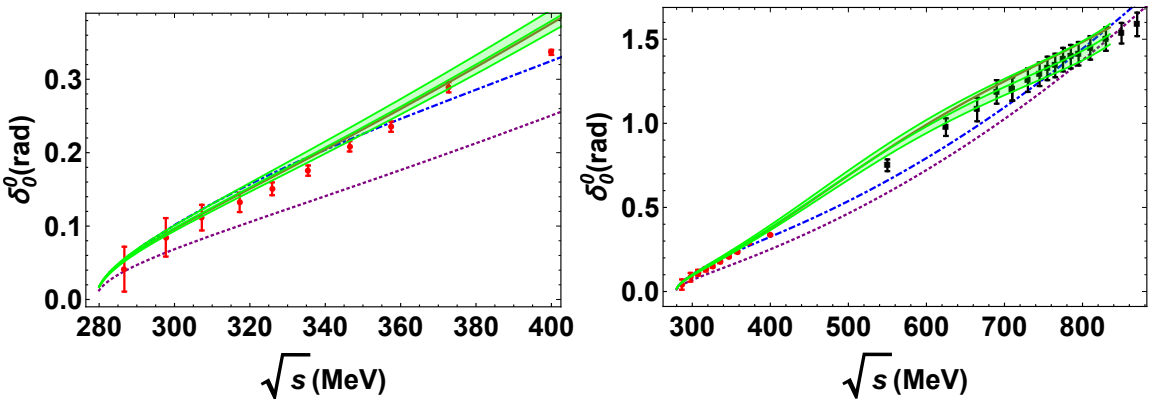

Figure 3: The $\pi\pi$ scattering phase shift as a function of the CM energy. In the left panel we show the results immediately above threshold, while the right panel shows the result up to $\sqrt{s} = 870$ MeV. In both panels the dashed purple line represents the standard χPT result and the dashed-dotted blue line is the combined result of diagrams (i) and (ii). This is to be compared to the red circles (black squares) that represent the data from Ref. [15] (Ref. [17]). The solid green and brown curves are results from the dispersive analyses of Refs. [4, 16] respectively. The green shaded band is a parameterization of the error reported in Ref. [4].

Adding the s-channel σ brings the total phase shift closer to these data, although there is somewhat of a difference in the curvature at higher energies between the data and the LO χPT_S amplitude.

The t- and u-channel σ-meson poles are part of the NLO χPT_S $\pi\pi$ amplitude. Unlike the standard χPT amplitude, Eq. (4.1) does not respect crossing symmetry—even before the isospin projection is made. The NLO graphs (iii) and (iv), with a dressed σ propagator, restore crossing symmetry. The additional amplitude in the $I = 0$ channel is:

$$\Delta T^{I=0}(s,t,u) = -\frac{4\, c_{1d,r}^2}{F^2}\left(\frac{(t-2m_\pi^2)^2}{t-m_{S,r}^2-2f_{2p,r}t^2-c_{1d,r}^2\tilde{\Sigma}(t)}+\frac{(u-2m_\pi^2)^2}{u-m_{S,r}^2-2f_{2p,r}u^2-c_{1d,r}^2\tilde{\Sigma}(u)}\right). \tag{4.3}$$

The t- and u-channel σ-pole have a markedly smaller effect on the $I = 0$ S-wave phase shift than does the s-channel one [13]: consistent with these graphs being NLO in the χPT_S amplitude. We sacrifice crossing symmetry so our EFT encodes the hierarchy of mechanisms for $4m_\pi^2 < s < M_\sigma^2$.

As already observed, our amplitude violates unitarity. Since the standard χPT $\mathcal{O}(p^2)$ amplitude is the largest piece of the S-wave phase shift it drives this violation. It violates the simplest consequence of unitarity already for $\sqrt{s}$ slightly below 700 MeV [18]. Furthermore, the size of the phase shift for $\sqrt{s} \geq 600$ MeV implies that the $\mathcal{O}(p^4)$ χPT amplitude will already produce marked corrections to the LO result in that region, so the results here cannot be trusted beyond $\sqrt{s} = 600$ MeV.

5. $\gamma\gamma \to \pi^0\pi^0$ cross section and pion polarizabilities in χPT_S

There are no $\mathcal{O}(p^2)$ (tree-level) contributions to the reaction $\gamma\gamma \to \pi^0\pi^0$. Note also that the σ is not charged, so minimal substitution does not generate any tree-level couplings between it and photons. This process therefore must involve pion-loop contributions, and in χPT_S these come in two varieties: diagrams with a σ pole and diagrams without such a pole.

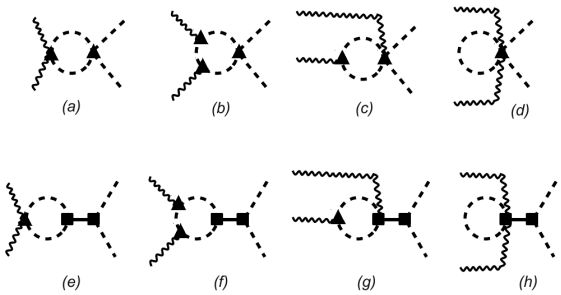

Figure 4: The leading-order diagrams for the process $\gamma\gamma \to \pi^0\pi^0$ in χPT_S. The upper four correspond to standard χPT while the lower four appear additionally in χPT_S. The wavy lines are photons. The direction of time is to the right.

The top line of Fig. 4 shows the $\mathcal{O}(p^4)$ contributions to the process $\gamma\gamma \to \pi^0\pi^0$ of the first type. These are the standard χPT graphs at this order. In χPT_S the bottom four graphs—again with a dressed σ propagator—are part of the LO amplitude if we consider the region $s \sim M_\sigma^2$.

The Ward identity for the upper four standard χPT diagrams of Fig. 4 has been verified in Ref. [19]. We derived the Ward identity for the bottom four graphs in Ref. [13].

Turning now to the $\gamma\gamma \to \pi^0\pi^0$ cross section, the amplitude for the top four standard χPT graphs of Fig. 4 is evaluated in Ref. [19] and here we simply recycle their results for that part of the amplitude. The cross-section data for $\gamma\gamma \to \pi^0\pi^0$ process have been measured by The Crystal Ball Collaboration and reported in Ref. [20]. The scattering cross section for $\gamma\gamma \to \pi^0\pi^0$ measured there can be expressed as

$$\sigma = \frac{1}{2} 3.2\pi \left[\frac{1}{256\pi^2 s} \sqrt{1 - \frac{4m_\pi^2}{s}} \left(\frac{s^2}{2} + s m_\pi^2 + m_\pi^4 \right) \left(|H_{\chi PT}(s) + H_\sigma(s)|^2 \right) \right], \tag{5.1}$$

where the standard χPT and additional part of the amplitude that arise in χPT_S ($H_\sigma(s)$) are:

$$H_{\chi PT}(s) = -\frac{1}{8\pi^2} \frac{2e^2}{F^2} \frac{s - m_\pi^2}{s} \left\{ 1 + \frac{m_\pi^2}{s} \left[\ln\left(\frac{x_+}{x_-} \right) - i\pi \right]^2 \right\}, \tag{5.2}$$

and

$$\begin{aligned} H_\sigma(s) = \frac{2c_{1d,r}^2 e^2}{F^2\pi^2} \Bigg[\frac{1}{4s^2} \Bigg\{ -2m_\pi^2 (s + 2m_\pi^2 \log(m_\pi^2)) + \frac{1}{3} \Bigg(18 m_\pi^2 s - 2s^2 + 12 m_\pi^4 \log(m_\pi^2) \\ + 12 m_\pi^2 (s - 2m_\pi^2) \left[Li_2\left(\frac{1}{x_+} \right) + Li_2\left(\frac{1}{x_-} \right) \right] \Bigg) \Bigg\} - \frac{1}{3} \Bigg] \left(\frac{(s - 2m_\pi^2)}{s - m_{S,r}^2 - 2 f_{2p,r} s^2 - c_{1d,r}^2 \tilde{\Sigma}(s)} \right), \end{aligned} \tag{5.3}$$

with $x_\pm = \frac{1}{2} \pm \frac{1}{2}\sqrt{1 - \frac{4m_\pi^2}{s}}$, and Li_2 representing the dilogarithm function.

In Fig. 5, the left graph shows the $\gamma\gamma \to \pi^0\pi^0$ cross section due to the lower four graphs of Fig. 4, those that involve the σ-meson pole. The bump seen there is inherited by the result for the total cross section: the dashed-dotted blue curve in the right panel, which has some signal of the σ resonance near 400 MeV. There is a good match between the LO χPT_S $\gamma\gamma \to \pi^0\pi^0$ cross

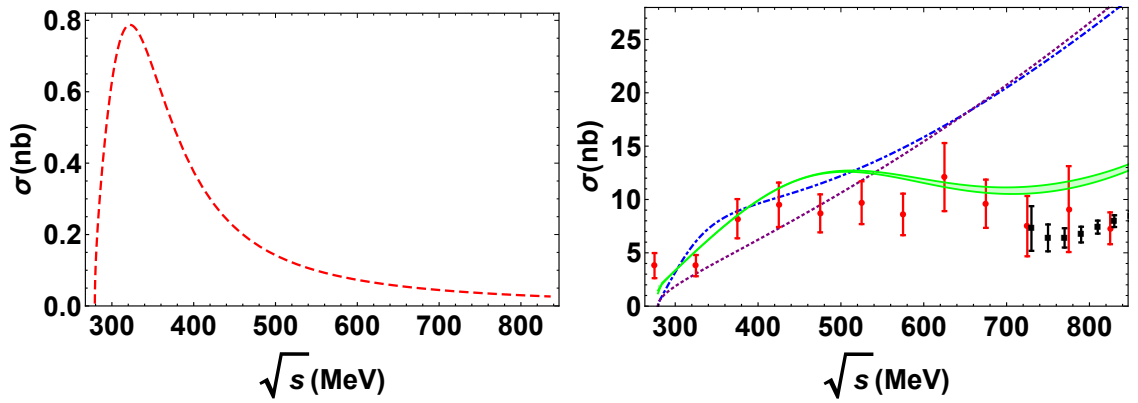

Figure 5: The $\gamma\gamma \to \pi^0\pi^0$ cross section as a function of the CM energy for $|\cos\theta| \leq 0.8$, where θ is the CM scattering angle. The dashed red curve in the left panel is the contribution from only the bottom graphs of Fig. 4. Meanwhile the dotted purple curve in the right panel is the leading contribution in χPT, i.e., the top graphs in Fig. 4. The dashed-dotted blue curve in the right panel is the total combined result at LO in χPT_S. Experimental data are from Ref. [20] (red circles) and Ref. [21] (black squares). The green band represents the once-subtracted result obtained in Ref. [22] from a dispersive Roy-equation analysis.

section and that obtained in a Roy-equation treatment of this reaction (with one subtraction) [22] up to $\sqrt{s} \approx 550$ MeV. The calculation of Ref. [22] is represented in Fig. 5 by the green band. The enhancement that we attribute to the s-channel σ-meson pole is slightly visible in the data (red circles) from Ref. [20]. Our result for the total cross section agrees with this data to within 1.5 standard deviations up to $\sqrt{s} \approx 550$ MeV.

At higher energies our LO result and the Roy-equation result of Ref. [22] have very different energy dependence. As already discussed in Sec. 4, the absence of $\pi\pi$ loop graphs means our LO amplitude is not correct once the $\pi\pi$ phase shift becomes significant, and the energy dependence obtained at LO in this theory is not a good match for the Roy-equation parameterization once $\sqrt{s} \geq 600$ MeV. This also means we cannot describe the higher-statistics, higher-energy data on $\gamma\gamma \to \pi^0\pi^0$ obtained in Ref. [21]. Those data are represented by the black squares in Fig. 5.

Finally, we examine the pion electromagnetic polarizabilities. The $(\alpha_1 - \beta_1)_{\pi^0}$ difference of dipole and $(\alpha_2 - \beta_2)_{\pi^0}$ difference of quadrupole polarizabilities are defined [19] through the expansion of the amplitude $H(s)$=$H_{\chi PT}(s)$+$H_\sigma(s)$ about s=0 as

$$\frac{1}{4\pi m_\pi} H(s) = (\alpha_1 - \beta_1)_{\pi^0} + \frac{s}{12}(\alpha_2 - \beta_2)_{\pi^0} + \mathcal{O}(s^2) \,. \tag{5.4}$$

In Table 1, we present our values of polarizabilites along with those from standard χPT one-loop [$\mathcal{O}(p^4)$], two-loop [$\mathcal{O}(p^6)$], and dispersion-relation calculations. We see from Table 1 that our calculation does capture some physics beyond the standard one-loop calculation, and seems to incorporate some of the two-loop physics that gives large corrections to both $(\alpha_1 - \beta_1)_{\pi^0}$ and $(\alpha_2 - \beta_2)_{\pi^0}$. However, a calculation with $f_{2p,r} = 0$ (and $c_{1d,r}$ re-adjusted to again reproduce the σ width) bridges half the gap between the $\mathcal{O}(p^4)$ and $\mathcal{O}(p^6)$ polarizabilities. Of course, this is at the cost of an unphysically large $\pi\pi$ and $\gamma\gamma \to \pi\pi$ cross section.

Table 1: The dipole and quadrupole polarizabilities in units of 10^{-4} fm^3 and 10^{-4} fm^5. The second and third columns contain the standard χPT one-loop and two-loop results from Ref. [19] and Ref. [23] respectively. The fourth column contains the results from dispersion-relation calculations [23] The last column is our χPT$_S$ result at one-loop.

Polarizabilities	χPT to one-loop	χPT to two-loop	Disperson relations	χPT$_S$ at one-loop
$(\alpha_1 - \beta_1)_{\pi^0}$	-0.98[19]	-1.9[23]	-1.6[23]	-1.1
$(\alpha_2 - \beta_2)_{\pi^0}$	20.37[19]	37.6[23]	39.7[23]	21.6

6. Conclusion

In this paper we have shown that an EFT in which standard χPT is augmented by the addition of a light scalar field, worked out initially by Soto, Talavera, and Tarrús in Ref. [9], provides a consistent and accurate leading-order description of the σ-meson pole, the isoscalar $\pi\pi$ scattering length, and the data for $\pi\pi$ scattering and $\gamma\gamma \to \pi^0\pi^0$ up to center-of-mass energies ≈ 500 MeV. This obviates the need for the inconsistent treatment of the $\pi\pi$ amplitude in $\gamma\gamma \to \pi^0\pi^0$ adopted in Ref. [10]. We also found that the analytic result of Refs. [9, 11] for the σ-meson width is too large by a factor of two.

We resum the scalar-meson's self-energy in the vicinity of the resonance. This gives the leading contribution to the σ's width in χPT$_S$. It also mandates a modification to the σ propagator that makes it $\sim s^{-2}$ for s far from the σ pole. This produces quite a weak σ effect on the real s-axis, which is where experiments are done.

Lastly, we observe that the power counting in which our leading-order calculation was derived has some issues if its accuracy is reviewed *a posteriori*. For example, the s-channel σ pole is nominally the LO mechanism [$\mathcal{O}(p^0)$] for $s \sim M_\sigma^2$. However, the results for $\pi\pi$ scattering show that—after all the parameters are chosen—that s-channel σ pole is a fairly small correction to the $\mathcal{O}(p^2)$ χPT amplitude in this region.

Acknowledgments

This work was supported by the US Department of Energy under grant number DE-FG02-93ER-40756. AT thanks the Mildred Mickel Hoover Dean's fellowship for facilitating his participation in this meeting.

References

[1] J. R. Peláez, *From controversy to precision on the sigma meson: a review on the status of the non-ordinary $f_0(500)$ resonance*, Phys. Rept. **658**, 1 (2016). [arXiv:1510.00653 [hep-ph]].

[2] K. A. Olive *et al.*, *Review of Particle Physics*, Chin. Phys. C **38**, 090001 (2014).

[3] I. Caprini, G. Colangelo, and H. Leutwyler, *Mass, and width of the lowest resonance in QCD,* Phys. Rev. Lett. **96**, 132001 (2006). [hep-ph/0512364].

[4] G. Colangelo, J. Gasser, and H. Leutwyler, $\pi\pi$ *scattering,* Nucl. Phys. B **603**, 125 (2001). [hep-ph/0103088].

[5] R. Garcia-Martin, R. Kaminski, J. R. Peláez, and J. Ruiz de Elvira, *Precise determination of the f0(600), and f0(980) pole parameters from a dispersive data analysis,* Phys. Rev. Lett. **107**, 072001 (2011). [arXiv:1107.1635 [hep-ph]].

[6] B. Moussallam, *Couplings of light I=0 scalar mesons to simple operators in the complex plane,* Eur. Phys. J. C **71**, 1814 (2011). [arXiv:1110.6074 [hep-ph]].

[7] R. J. Crewther and L. C. Tunstall, *Status of Chiral-Scale Perturbation Theory,* in proceedings of *the 8th International workshop on the Chiral Dynamics* PoS CD **15**, 132 (2015) [arXiv:1510.01322 [hep-ph]].

[8] M. Golterman and Y. Shamir, *Low-energy effective action for pions and a dilatonic meson,* Phys. Rev. D **94**, no. 5, 054502 (2016). [arXiv:1603.04575 [hep-ph]].

[9] J. Soto, P. Talavera, and J. Tarrus, *Chiral Effective Theory with A Light Scalar, and Lattice QCD,* Nucl. Phys. B **866**, 270 (2013). [arXiv:1110.6156 [hep-ph]].

[10] L. Ametller and P. Talavera, *Lowest resonance in QCD from low-energy data,* Phys. Rev. D **89**, no. 9, 096004 (2014); [arXiv:1402.2649 [hep-ph]]; Phys. Rev. D **92**, 074008 (2015). [arXiv:1504.06505 [hep-ph]].

[11] M. Hansen, K. Langæble and F. Sannino, *Extending Chiral Perturbation Theory with an Isosinglet Scalar,* Phys. Rev. D **95**, no. 3, 036005 (2017). [arXiv:1610.02904 [hep-ph]].

[12] J. Gasser and H. Leutwyler, *Quark Masses,* Phys. Rept. **87**, 77 (1982).

[13] A. Thapaliya and D. R. Phillips, *The reactions* $\pi\pi \to \pi\pi$ *and* $\gamma\gamma \to \pi\pi$ *in* χPT *with an isosinglet scalar resonance,* Eur. Phys. J. A **53**, no. 10, 206 (2017).

[14] P. C. Bruns, *On the sigma sigma term,* arXiv:1610.00119 [nucl-th].

[15] J. R. Batley *et al.* [NA48-2 Collaboration], *Study of the decay phi —> pi0 pi0 gamma with the KLOE detector,* Eur. Phys. J. **C70**, 635-657 (2010).

[16] R. Garcia-Martin, R. Kaminski, J. R. Peláez, J. Ruiz de Elvira and F. J. Yndurain, *The Pion-pion scattering amplitude. IV: Improved analysis with once subtracted Roy-like equations up to 1100 MeV,* Phys. Rev. D **83**, 074004 (2011) [arXiv:1102.2183 [hep-ph]].

[17] S. D. Protopopescu *et al.*, *A pi pi PHASE SHIFT ANALYSIS FROM REACTIONS pi+ p —> pi+ pi- DELTA++ AND pi+ p —> K+ K- DELTA++ at 7.1-GeV/c* in proceedings of *Proc. Int. Conf. on Experimental Meson Spectroscopy,* Amer. Inst. Phys., 1972. p. 17-58.

[18] J. F. Donoghue, E. Golowich, B. R. Holstein, *Dynamics of the Standard Model*, p. 180, Cambridge University Press, Cambridge, 1992.

[19] J. F. Donoghue, B. R. Holstein, and Y. C. Lin, *The Reaction gamma Gamma —> pi0 pi0, and Chiral Loops,* Phys. Rev. D **37**, 2423 (1988).

[20] H. Marsiske *et al.* [Crystal Ball Collaboration], *A Measurement of* $\pi^0\pi^0$ *Production in Two Photon Collisions,* Phys. Rev. D **41**, 3324 (1990).

[21] S. Uehara *et al.* [Belle Collaboration], *High-statistics measurement of neutral pion-pair production in two-photon collisions,* Phys. Rev. D **78**, 052004 (2008). [arXiv:0805.3387 [hep-ex]].

[22] M. Hoferichter, D. R. Phillips, and C. Schat, *Roy-Steiner equations for gamma gamma -> pi pi,* Eur. Phys. J. C **71**, 1743 (2011) [arXiv:1106.4147 [hep-ph]].

[23] J. Gasser, M. A. Ivanov, and M. E. Sainio, *Low-energy photon-photon collisions to two-loops revisited,* Nucl. Phys. B **728**, 31 (2005). [hep-ph/0506265].